

Article

Microstructural Analysis and Tribological Behavior of Ti-Based Alloys with a Ceramic Layer Using the Thermal Spray Method

Madalina Simona Baltatu ¹, Petrica Vizureanu ^{1,*} , Andrei Victor Sandu ^{1,2} ,
Corneliu Munteanu ³  and Bogdan Istrate ³ 

¹ Department of Technologies and Equipments for Materials Processing, Faculty of Materials Science and Engineering, Gheorghe Asachi Technical University of Iasi, Boulevard D. Mangeron, No. 51, 700050 Iasi, Romania; cercel.msimona@yahoo.com (M.S.B.); sav@tuiasi.ro (A.V.S.)

² Romanian Inventors Forum, Iasi. Sf. P. Movila 3, 700089 Iasi, Romania

³ Mechanical Engineering, Mechatronics and Robotics Department, Mechanical Engineering Faculty, Gheorghe Asachi Technical University of Iasi, Boulevard D. Mangeron, No. 63, 700050 Iasi, Romania; cornelmun@gmail.com (C.M.); bogdan_istrate1@yahoo.com (B.I.)

* Correspondence: peviz2002@yahoo.com

Received: 6 November 2020; Accepted: 9 December 2020; Published: 12 December 2020



Abstract: The present article focuses on a recently developed new system of alloys (Ti15MoSi) coated with ZrO₂. The thin coatings deposition of ZrO₂ on titanium alloys can be a solution to improve their corrosion resistance, biocompatibility, and to extend their long life with the human tissue. In order to improve the corrosion resistance, atmospheric plasma spraying coatings with zirconia have been performed. These coatings present a homogenous aspect with very few cracks. The novelty of the research is that zirconia is much stable in the simulated body fluids and presents no harm effects to the healing process of the bone. To analyze the thin coatings deposition, mechanical properties, chemical structure, and corrosion resistance were examined by a modulus of elasticity, X-ray diffraction (XRD), scanning electron microscopy-energy-dispersive X-ray spectroscopy (SEM-EDS), and linear polarization. The results reveal that Young's modulus shows a low value (51 GPa for Ti15Mo0.5Si-ZrO₂ and 48 GPa for Ti15Mo-ZrO₂) and the XRD patterns show the presence of β-Ti and ZrO₂ phases having a tetragonal crystalline structure. The research highlighted the morphological aspect of zirconia coatings on the new alloy titanium substrate, being an adherent compact coating with significantly improved corrosion resistance. Moreover, the mechanical properties are similar to the biological bone, which will avoid the stress shielding of the implant with bone tissue.

Keywords: Ti-based alloys; thin coatings; atmospheric plasma spray (APS); scanning electron microscopy (SEM); energy-dispersive X-ray spectroscopy (EDAX)

1. Introduction

Health is a very important issue and researchers work hard to improve alloys for medical applications [1]. Therefore, it is desired to improve both the classic technologies of implant execution and the technologies of biomaterials synthesis, from which they are executed, with the ultimate goal of promoting a new generation of multifunctional implants with long-term performance [2].

Biomaterials must be tolerated by the body for a long time (decades), and therefore, must meet the functional requirements according to the medical specifications [3], in which they are to be used [4]. The biomaterials initially used for the manufacture of implantable devices, in contact with elements of biological systems, were materials of general use, which met to a greater or lesser extent the specific requirements of the medical field, being known as first generation biomaterials [5].

The materials used for medical applications must include biocompatible elements with mechanical properties suitable for the system that replaces it and a high corrosion resistance [6]. A biomaterial is a material used for the permanent or partial replacement of a living organ or system or for functioning in close contact with active tissues. The main purpose is the use of biomaterials to repair human tissues [7]. Artificial materials come in direct contact with the body or are introduced into the body, which requires them to have certain characteristics in order to be accepted [8].

In recent years, second-generation biomaterials have emerged, which are synthesized given the existence and control of physical, chemical, and biological processes at the implant/tissue interface, so that normal cellular processes are stimulated [9].

Titanium and its alloys have attracted the attention of scientists [10] and are of great interest for use in medical applications, since they have important characteristics, which are required by implant materials including good mechanical properties (lower modulus of elasticity than stainless steel or CoCr alloys, fatigue strength, strength corrosion), high biocompatibility, and a good corrosion resistance [11,12]. These materials have multiple uses in orthopedics, dentistry, maxillofacial surgery, and cardiovascular surgery [10,12].

The most widely used alloy and among the first titanium alloys used is Ti6Al4V [9]. Many researchers have argued that this alloy causes allergic reactions in the human body. Since the biocompatibility of the patient's health is placed first, researchers have developed and investigated the second generation of titanium alloys with alloying elements such as Mo, Ta, Zr, Si, etc. [13–17]. Compared with vanadium and aluminum, the elements have shown a high biocompatibility. Ideally, non-toxic elements should be selected as alloying elements in developing a biomedical alloy [18].

The use of zirconia ceramics as orthopedic implants and dental applications [19,20], has received great attention due to their excellent properties. The papers in the field [21–23] highlight the layers of ZrO_2 exhibiting an excellent wear resistance due to its phase constituent and a better corrosion resistance.

Vilardell et al. [24] performed comparative studies for different deposition methods (APS > HVOF > CS), and showed that the APS method has a better cell adhesion and proliferation [25]. In the field of coating techniques, there are several mentioned methods of deposition such as atmospheric plasma spraying, as well as physical and chemical vapor deposition (PVD and CVD processes) [26]. Nevertheless, PVD and CVD techniques have drawbacks of being more expensive and laborious than the proposed coating deposition. The plasma jet deposition process is considered to be the most versatile of all thermal spray deposition processes. The process uses argon (Ar) as the primary gas, hydrogen (H_2) as the secondary gas, and nitrogen (N_2) as the carrier gas of the zirconia powder [27]. The powder melts at contact with the plasma jet, reaching values at very high temperatures and exceeding the melting temperature of any material. The powder is injected into the flame, melted, and accelerated to the substrate [28,29].

Even if the APS deposited layers have a good adherence, this method is used very little. In this paper, the thin coatings deposition of ZrO_2 by the APS method on four titanium alloys is presented. The objectives of this study were to determine (1) the morphological study of the layers, (2) the mechanical properties obtained by micro-indentation; and (3) the electrochemical tests in specific environments.

The aim of the study is to highlight some zirconia coatings properties deposited on new Ti-based alloys. The influence of the alloying elements is exerted directly on the properties of the final material and the optimum percentage must be carefully chosen. We selected a system based on Ti-Mo-Si, since Titanium is considered an element with extremely low toxicity for the human body. In addition, its use in medical applications is due to a very good interaction with the host bone, Molybdenum, which is a beta-stabilizing element with a low degree of toxicity and in 15–20 wt.%, Mo could lead to the decrease of the modulus of elasticity, while Silicon increases corrosion resistance and fluidity during casting. Ti-Mo-Si with good mechanical properties and low corrosion resistance are suitable for medical applications as orthopedic implants.

2. Materials and Methods

2.1. Ti-Mo-Si Substrate Alloys

As the substrate material for deposition, a new titanium, silicon, and molybdenum alloy was used based on an original recipe, according to Table 1.

Table 1. Average elemental compositions obtained by energy dispersive X-ray spectroscopy analysis for the base alloy.

Sample		Ti (wt.%)	Mo (wt.%)	Si (wt.%)
S1	Average	84.5	15.5	-
	Stdev	±0.2	±0.2	-
S2	Average	84.7	15.0	0.3
	Stdev	±0.2	±0.3	±0.1
S3	Average	83.8	15.3	0.9
	Stdev	±0.9	±0.2	±0.1
S4	Average	83.9	15.1	1.0
	Stdev	±0.6	±0.5	±0.1

The Ti-Mo-Si based alloys were obtained in a vacuum arc remelting (VAR) MRF ABJ 900 equipment, from high purity elements: Ti (99% purity), Mo (99% purity), and Si (99% purity) supplied by Alfa Aesar, Thermo Fisher Scientific (Waltham, MA, USA). The obtained ingots were then cut into disc samples with a diameter of 10 mm and a thickness of 2 mm for specific tests.

2.2. Atmospheric Plasma Jet Deposition

Four samples of Ti-Mo-Si substrate alloys, coated with ZrO₂ were prepared. The powders were manufactured by Alfa Aesar, Thermo Fisher Scientific. The Sulzer Metco 9MCE plasma jet deposition facility was applied. The coatings parameters are shown in Table 2. The substrates for depositions were prepared in the following way: The samples were cut to the required dimensions, sandblasted by the casting sand, cleaned by ethyl alcohol, and positioned on a support plate.

Table 2. Deposition parameters of ceramic coatings.

Powder	Gun Type	Ar		H ₂		Electric		Powder Feeder 9 MP			Spraying Distance [mm]
		Pressure [MPa]	Gas Flow [NLPM]	Pressure [MPa]	Gas Flow [NLPM]	DC [A]	DC [V]	Carrier Gas Flow [NLPM]	Air Pressure [MPa]	Quantity [g/min]	
ZrO ₂	9 MB	350	40	350	6.7	400	70–80	5.1	150	126	105

The zirconia powder is in accordance with the producer catalogue, which presents a spherical shape in the range of 30–50 µm.

2.3. Morphological and Structural Analysis

The morphological and compositional analysis was performed with X-ray energy dispersion SEM Quanta 200 3D Dual Beam and Vega 2 LSH Tescan Brno, Czech Republic. The investigation was necessary to highlight the proportions obtained between the pure chemical elements and investigation of morphological analysis. For the based materials microstructure, the samples were grounded with abrasive discs with granulation between 150–2500 MPi, polished with alumina suspension (1–6 µm), cleaned with alcohol, and then ultrasonically cleaned in ethyl alcohol for 10 min. For the microstructural analysis, the experimental samples were etched with a 10 mL HF, 5 mL HNO₃, and 85 mL H₂O solution.

Phase determination was performed by the qualitative X-ray diffraction analysis using an Expert PRO MPD facility from Panalytical (Almelo, The Netherlands), with a Copper X-ray tube (Kα-1.54051°). The processing of the obtained data was done with the Highscore Plus software, and then

the diffractograms were depicted. Samples with dimensions of $10 \times 10 \times 5 \text{ mm}^3$ were used to determine the constituent phases. X-ray diffractions (XRD, Panalytical, Almelo, The Netherlands) were performed using an Xpert PRO MPD 3060 facility from Panalytical (Almelo, The Netherlands), with a Cu X-ray tube ($K\alpha = 1.54051 \text{ \AA}$), 2θ : $10\text{--}90^\circ$, step size: 0.13° , time/step: 51 s, and a scan speed of $0.065651^\circ/\text{s}$.

2.4. Micro-Indentation Test

Tribological properties of coated alloys were analyzed through micro-scale indentation tests and performed by the CETR UMT-2 Tribometer (Schaefer (CETR, Campbell, CA, USA)). For the micro-indentation test, semi disc-type samples with a diameter of 20 mm and a thickness of 2 mm were used. A Rockwell diamond tip indenter, with a 120° opening angle at the edge of the indenter was applied. The accepted standard values of Rockwell's indenter dimensional parameters were as follows: Radius is $200 \pm 10 \text{ }\mu\text{m}$; angle is $120 \pm 0.35^\circ$; deviation from profile is $\pm 2 \text{ }\mu\text{m}$. For a better accuracy, three determinations were performed on the surface of each sample to obtain Young's modulus. The indentation method consisted of a progressive increase of the indentation force from 0 to 5 N and the return to the initial value. The capacitive sensor along with the force sensor allowed obtaining the typical indentation diagram (force-deformation). The CETR-UMT Test Viewer is the software used for micro-indentation.

2.5. Electrochemical Analysis

The corrosion of a biomaterial is determined by the aggressive nature of the biological fluids. In order to determine the corrosion potential on the elaborated titanium alloys, it is necessary to research them through these potentially dynamic and potentiostatic tests in biologically simulated environments [30].

A type of simulated physiological solution was prepared, currently used in the literature for the study of alloy corrosion used in orthopedic prostheses or in dentistry, respectively: Ringer's solution. Ti-Mo-Si coated samples have been tested in Ringer's solution at 37°C with the following composition (1):



The determination of corrosion potential and tracing of linear polarization curves will be performed with an electrochemical system PARSTAT 4000-Princeton Applied Research, USA. The potentiostat has special facilities for the precise determination of the polarization resistance, the recording of the corrosion potential for long periods of time, and tests on the corrosion in points.

The main operating parameters of the appliance are: Maximum working potential = $\pm 30 \text{ V}$, maximum output current = $\pm 1 \text{ A}$, and maximum bias voltage = $\pm 15 \text{ V}$. For electrochemical impedance measurements, the maximum frequency is 100 kHz and the minimum frequency is 1 mHz. An important advantage for potentiodynamic measurements with this device is that the scanning speed of the electrode potential can be increased up to 20.000 mV/s . The acquisition of the experimental data was done with the same software, VoltaMaster 4.

3. Results and Discussion

3.1. Microstructural Analysis

The zirconia powder was analyzed by the EDS system before deposition (Figure 1). The nominal range of powder was measured and the values are in the range of 30 to $50 \text{ }\mu\text{m}$. Figure 2 presents the measured powder morphology.

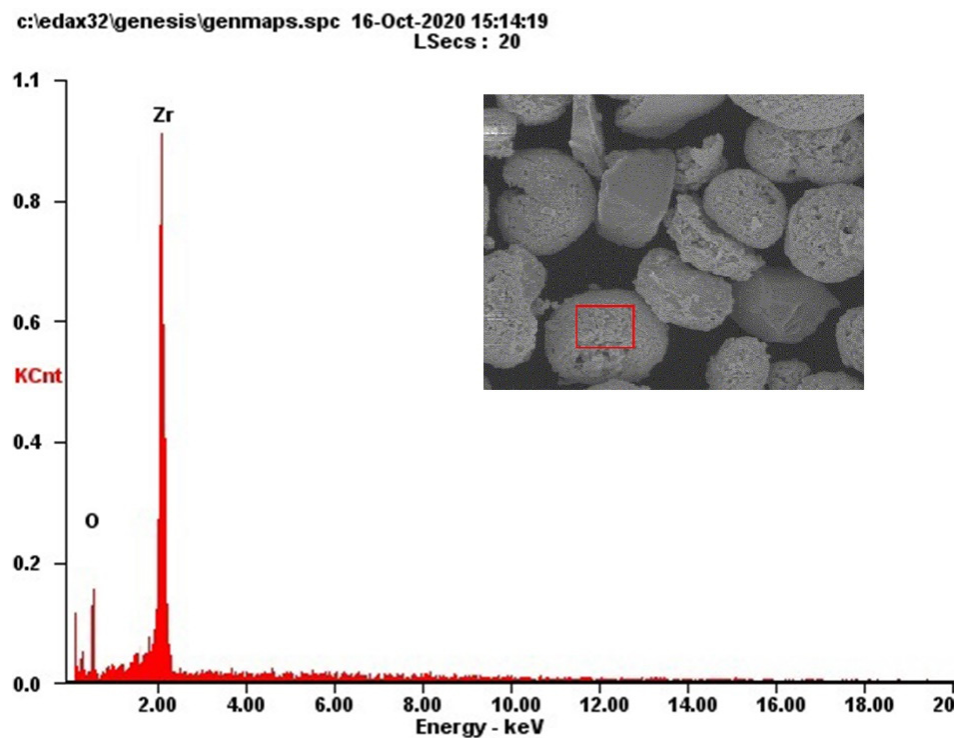


Figure 1. EDS spectrum of the powder morphology.

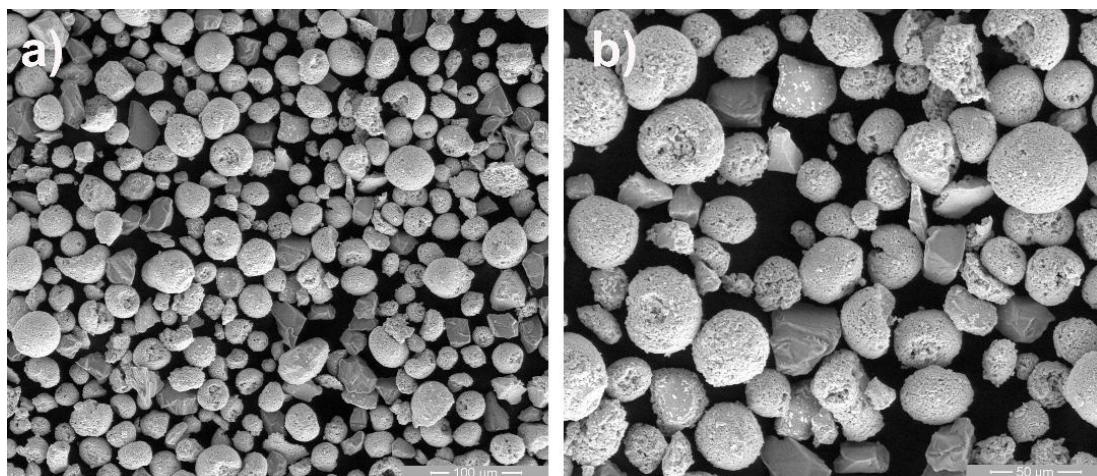


Figure 2. Micrographs of the powder morphology: (a) 500× magnification; (b) 1000× magnification.

After obtaining the TiMoSi samples and before being coated, the alloys were grounded and chemically etched to study the microstructure. The structural characterizations of the four alloys by optical microscopy are shown in Figure 3. The figures show the structure of TiMoSi substrate alloys with grain-specific aspects of titanium alloys and structures specific to the β alloys. The images obtained by optical microscopy for the analyzed TiMoSi alloys show a dendritic type structure with irregular grain boundaries, except for the Ti15Mo. The alloys Ti15Mo1.00Si and Ti20Mo0.75Si highlight very well the lamellar dendrites inside the β -type grains.

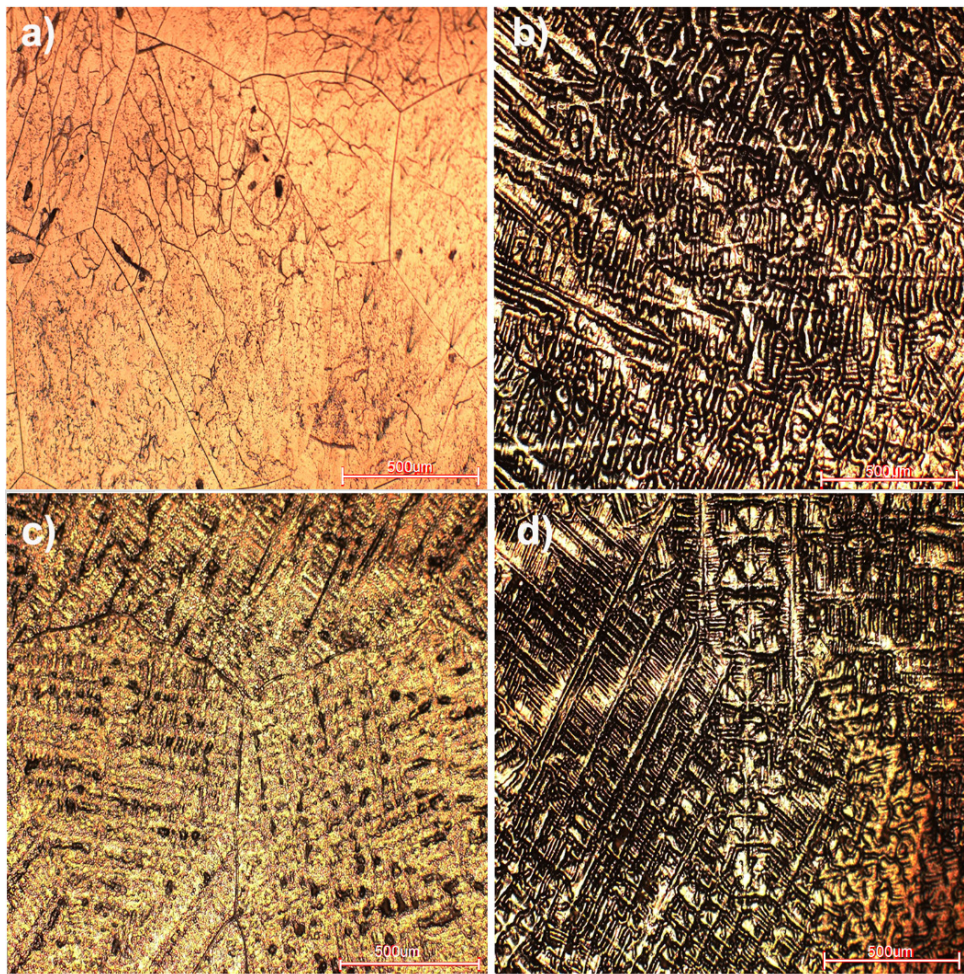


Figure 3. Light microscopy images of substrate materials: (a) S1; (b) S2; (c) S3; (d) S4.

Figure 4 shows the morphological aspects of the coated samples with ZrO_2 . Moreover, Table 3 presents the obtained EDX elemental compositions. Microstructures at different magnifications highlight the compactness of the coatings powers and the relatively low porosity. The use of the BSE detector at high magnification highlights the uniformity of the phases and the very small number of microcracks. The dark particles highlight the un-melted zirconia compounds and the mostly light colored area shows the uniformity of the zirconia oxide coating. The molten particles in the plasma jet struck with a high velocity the relatively low-temperature substrate or other particles that had been deposited previously, during the spraying process. They were stacked in a flat shape to form a smooth, dense surface structure with few pores. Some small cracks in the coatings were caused by the release of stress from the molten droplets in the flattening and rapid cooling process. At the same time, the semi-molten and unmolten particles in the plasma flame deform slightly, while striking the substrate. A part of the carrier gas can be retained in the obtained layer, resulting in pores of different sizes, respectively a heterogeneous rough microstructure. Table 4 presents the thickness of the coated layers, measured on SEM images.

The surface of the coatings had two different morphological features: (I) A smooth, dense morphology due to the fully-molten spraying powder; and (II) a loose, porous morphology which was mainly due to the spraying powder being inadequately molten during spraying. The melted particle of zirconia is deposited through the surface materials and forms a specific type of structure called “splats”, very common in these types of coatings.

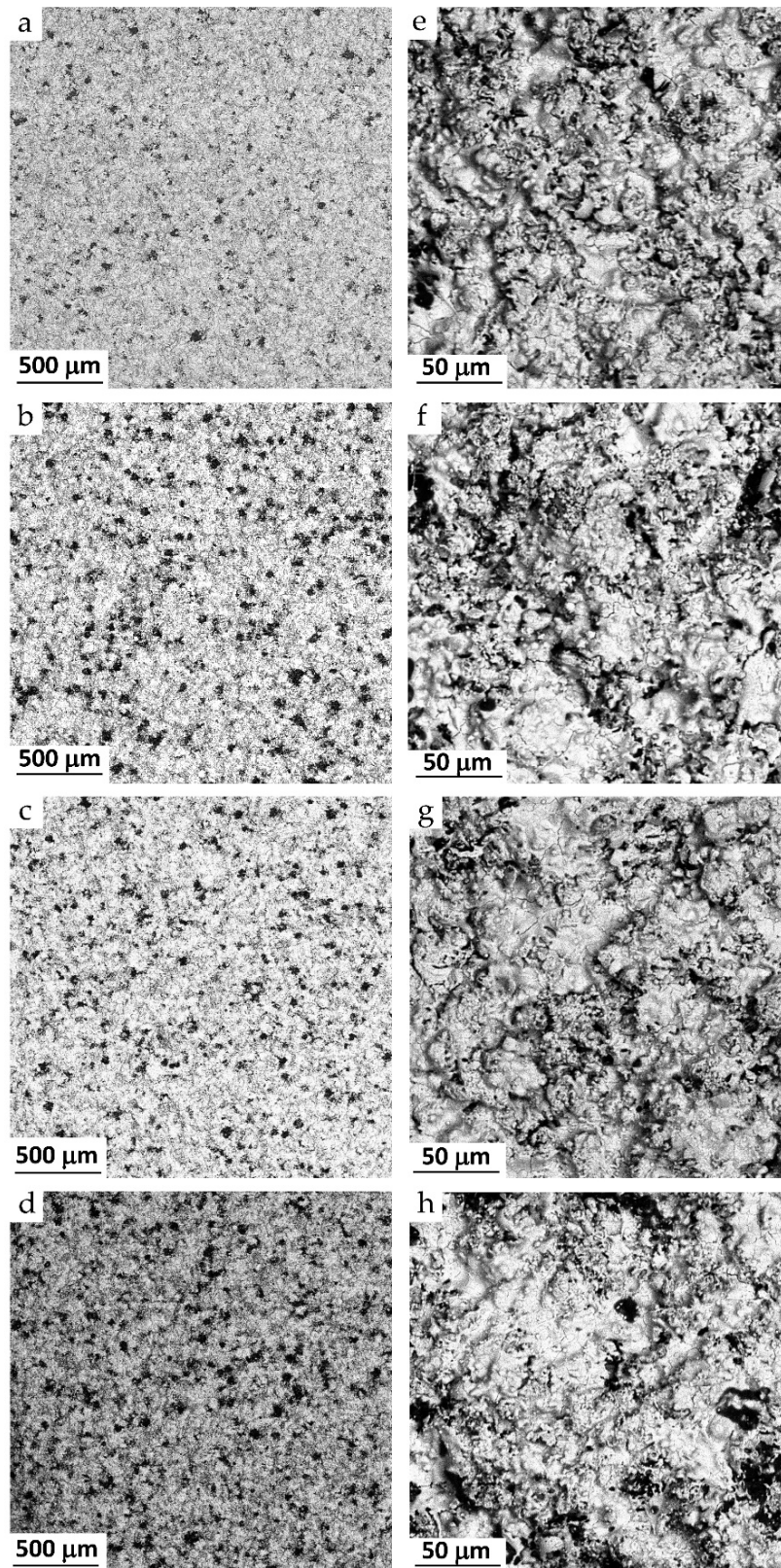


Figure 4. Morphological aspects of coated samples: (a) S1-ZrO₂; (b) S2-ZrO₂; (c) S3-ZrO₂; (d) S4-ZrO₂; (e) S1-ZrO₂; (f) S2-ZrO₂; (g) S3-ZrO₂; (h) S4-ZrO₂.

Table 3. Average elemental compositions obtained by energy dispersive X-ray spectroscopy analysis for the coated alloys.

Sample *		S1	S2	S3	S4
Average chemical composition	Zr (wt.%)	78.3 ± 0.3	74.3 ± 0.1	77.7 ± 0.1	70.8 ± 0.2
	O (wt.%)	21.7 ± 0.1	25.7 ± 0.2	22.3 ± 0.3	29.2 ± 0.2

* Ten EDX determinations were carried out in five different areas of the samples with dimensions of $10 \times 10 \times 5 \text{ mm}^3$, to obtain precise values for the composition.

Table 4. The thickness of the deposited layers.

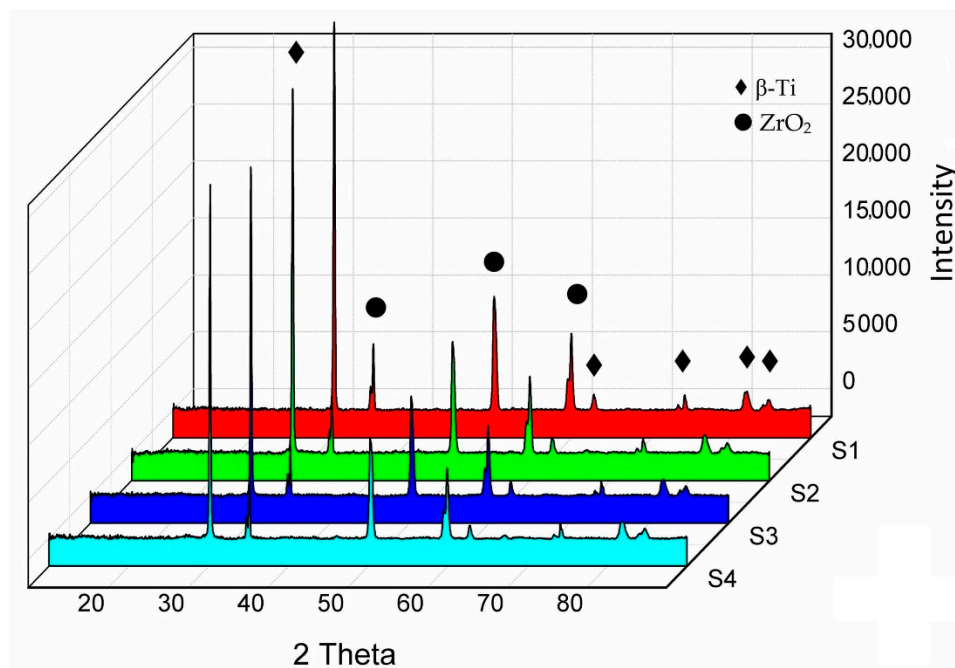
Sample	Layer Thickness (μm)
S1-ZrO ₂	83.30 ± 3.3
S2-ZrO ₂	82.56 ± 4.4
S3-ZrO ₂	85.77 ± 4.1
S4-ZrO ₂	84.30 ± 3.0

Researchers currently named the β titanium alloys as second generation titanium biomaterials. The reasons for these statements consist of the advantage of these alloys, a low modulus closer to the bone, and avoiding the stress shielding effect [9].

Titanium is an allotropic material, which comes in different forms with different properties: Up to a temperature of 882 °C, with a compact hexagonal structure α Ti and over 882 °C, β Ti, with a centered cubic structure [8].

Zirconia exists with tetragonal, monoclinic, rhombohedral, and cubic crystal structures, depending on stress, temperature, oxide additions, and pressure. Many mechanical and physical properties depend on the crystal structure, including the coefficient of thermal expansion (CTE) [31].

Figure 5 shows the XRD results of the coated alloys. For coated alloys, diffraction peaks for ZrO₂ appear at 38.4°, 55.5°, 69.5°, and 82.4°, the rest are β -Ti having a centered cubic structure.

**Figure 5.** XRD patterns for coated samples: S1-ZrO₂, S2-ZrO₂, S3-ZrO₂, S4-ZrO₂.

The variation of the α , $\alpha + \beta$, and β type phases on titanium alloys consists of the differences in the chemical composition of the constituent elements. In our case, the high percentage of β stabilizing

elements (Mo, Si) led to the formation of a β -type structure, highlighted in the structure analysis and XRD patterns.

3.2. Micro-Indentation Analysis

The micro-indentation analysis of coated samples is presented in Table 5. Mechanical properties, such as the elastic modulus, are very important criteria and underlie the selection of metallic materials used in orthopedics. The elastic modulus of the alloy used for implantation must be as close as possible to that of the human bone. Young's modulus shows values between 51.71 ± 0.1 and 48.27 ± 0.2 . These alloys reduce Young's modulus of the C.P. titanium (103–120 GPa) with 50% and are close to the cortical bone value (10–30 GPa). Compared with classical alloys (CoCrMo, Ti6Al4V), these alloys (S1-ZrO₂, S2-ZrO₂, S3-ZrO₂, S4-ZrO₂) present low Young's modulus, a stiffness suitable for orthopedic implants.

Table 5. Micro-indentation results.

Sample	Loading Deformation [N]	Release Deformation [μm]	Young's Modulus [GPa]	Stiffness [N/ μm]	Specimen Poisson Ratio
S1-ZrO ₂	13.5 ± 0.5	12.2 ± 0.5	48.3 ± 0.5	6.2 ± 0.5	0.23
S2-ZrO ₂	13.5 ± 0.5	9.7 ± 0.5	51.7 ± 0.5	5.8 ± 0.5	0.23
S3-ZrO ₂	13.5 ± 0.5	12.1 ± 0.5	49.1 ± 0.5	6.3 ± 0.5	0.23
S4-ZrO ₂	13.5 ± 0.5	11.4 ± 0.5	50.7 ± 0.5	6.2 ± 0.5	0.23

Five determinations were carried out in different areas of the samples with dimensions of $10 \times 10 \times 5 \text{ mm}^3$.

The coated samples showed a very low modulus of elasticity, close to that of the human bone (17–32 GPa), which makes them suitable for orthopedic applications.

3.3. Electrochemical Analysis

Figure 6 shows the Tafel plots for the coated samples studied in Ringer's solution and Table 6 shows the parameters of instantaneous corrosion in the same physiological environment.

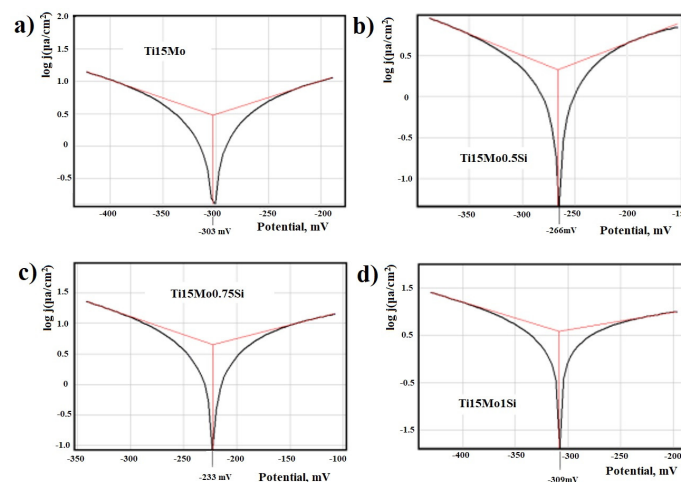


Figure 6. Tafel plots of coated samples investigated by corrosion testing in Ringer's solution: (a) S1-ZrO₂; (b) S2-ZrO₂; (c) S3-ZrO₂; (d) S4-ZrO₂.

The corrosion potential, E_{cor} , measured in relation to the saturated calomel electrode potential, is the potential at which the redox reactions on the alloy surface are at equilibrium. The rate of the oxidation reaction is equal to the rate of the reduction reaction and the intensity of the total current is zero. As the potential increases to more positive values, the rate of the oxidation reaction increases, while during the shift of the potential to negative values, the oxidation process is reduced and the metal becomes passivated. The presence of silicon seems to cause a decrease in the corrosion rate.

Table 6. Instantaneous corrosion parameters for coated samples in Ringer’s solution.

Sample	E_{cor} [mV]	$R_{p,r}$ [kohm.cm ²]	I_{cor} [A/cm ²]	V_{cor} [m/year]	$b_{a,r}$ [mV/dec.]	$b_{c,r}$ [mV/dec.]
S1-ZrO ₂	−303	11.18	3.033	29.30	194	−180
S2-ZrO ₂	−266	14.91	2.131	20.59	200	−192
S3-ZrO ₂	−223	7.49	4.458	43.09	222	−166
S4-ZrO ₂	−309	8.99	3.963	38.30	278	−152

The polarization resistors have high values, which are reflected in very low corrosion rates. The product of “corrosion” in the case of these alloys is mainly titanium oxide, TiO₂, which is insoluble and adherent to the surface of the alloy. The oxide layer on the surface protects the alloy from the aggressive absorption of electrolytic media. Given this, it can be admitted that artificial physiological environment samples do not corrode, but in reality, undergo a passivation process. Under these conditions, the V_{cor} parameter—called the corrosion rate—is actually the passivation speed. Except for two alloys, the passivation rates are of the same order of magnitude, the lowest passivation rate is being presented by the S2-ZrO₂ alloy.

4. Conclusions

In the present paper, zirconia coatings were made on the substrate of Ti15Mo, Ti15Mo0.5Si, Ti15Mo0.75Si, and Ti15Mo1.0Si. The coatings showed a uniform morphological aspect without microcracks, observing the presence of the β -Ti and ZrO₂ phases with a tetragonal crystalline structure. The dark particles highlight the un-melted zirconia compounds and the mostly light colored area shows the uniformity of the zirconia oxide coating.

The micro-indentation analysis revealed that Young’s modulus showed a low value (51.71 ± 0.1 and 48.27 ± 0.2), improving the Ti-based alloys by 50%. The instantaneous corrosion parameters for the coated samples in Ringer’s solution have very good values, with an oxide layer on the surface protecting the alloy from the aggressive absorption of electrolytic media.

Author Contributions: Writing—original draft preparation, investigation, M.S.B.; conceptualization, validation, P.V.; investigation, writing—review and editing, A.V.S.; methodology, visualization, C.M.; investigation, data curation, B.I. All authors have read and agreed to the published version of the manuscript.

Funding: This work was supported by a grant of the Romanian Ministry of Research and Innovation, CCCDI-UEFISCDI, project number PN-III-P1-1.2-PCCDI-2017-0239/60PCCDI 2018, within PNCDI III.

Conflicts of Interest: The authors declare no conflict of interest.

References

- Niinomi, M. Titanium Alloys. In *Encyclopedia of Biomedical Engineering*; Elsevier: Amsterdam, The Netherlands, 2019; pp. 213–224.
- Chen, Q.; Thouas, G.A. Metallic implant biomaterials. *Mater. Sci. Eng. R* **2015**, *87*, 1–57. [[CrossRef](#)]
- Bombac, D.M.; Brojan, M.; Fajfar, P.; Kosel, F.; Turk, R. Review of materials in medical applications. *RMZ Mater. Geoenviron.* **2007**, *54*, 471–499.
- Antoniac, I. (Ed.) *Handbook of Bioceramics and Biocomposites*; Springer: Berlin/Heidelberg, Germany, 2016; Available online: <https://www.springer.com/gp/book/9783319124599> (accessed on 15 September 2020).
- Song, Y.; Xu, D.S.; Yang, R.; Li, D.; Wu, W.T.; Guo, Z.X. Theoretical study of the effects of alloying elements on the strength and modulus of β -type bio-titanium alloys. *Mater. Sci. Eng. A* **1999**, *260*, 269–274. [[CrossRef](#)]
- Bermúdez, M.-D.; Carrión, F.J.; Martínez-Nicolás, G.; López, R. Erosion–corrosion of stainless steels, titanium, tantalum and zirconium. *Wear* **2005**, *258*, 693–700. [[CrossRef](#)]
- Sandu, A.V.; Baltatu, M.S.; Nabialek, M.; Savin, A.; Vizureanu, P. Characterization and mechanical properties of new TiMo alloys used for medical applications. *Materials* **2019**, *12*, 2973. [[CrossRef](#)]
- Geetha, M.; Singh, A.K.; Asokamani, R.; Gogia, A.K. Ti based biomaterials, the ultimate choice for orthopaedic implants—A review. *Mater. Sci.* **2009**, *54*, 397–425. [[CrossRef](#)]

9. Niinomi, M. Mechanical properties of biomedical titanium alloys. *Mater. Sci. Eng. A* **1998**, *243*, 231–236. [[CrossRef](#)]
10. Elias, C.N.; Lima, J.H.C.; Valiev, R.; Meyers, M.A. Biomedical applications of titanium and its alloys (Review). *Biol. Mater. Sci.* **2008**, *60*, 46–49. [[CrossRef](#)]
11. Baltatu, M.S.; Tugui, C.A.; Perju, M.C.; Benchea, M.; Spataru, M.C.; Sandu, A.V.; Vizureanu, P. Biocompatible titanium alloys used in medical applications. *Rev. Chim.* **2019**, *70*, 1302–1306. [[CrossRef](#)]
12. Minciuna, M.G.; Vizureanu, P.; Geanta, V.; Voiculescu, I.; Sandu, A.V.; Achitei, D.C.; Vitalariu, A.M. Effect of Si on the mechanical properties of biomedical CoCrMo alloys. *Rev. Chim.* **2015**, *66*, 891–894.
13. Baltatu, M.S.; Vizureanu, P.; Balan, T.; Lohan, M.; Tugui, C.A. Preliminary tests for Ti-Mo-Zr-Ta alloys as potential biomaterials. In Proceedings of the IOP Conference Series: Materials Science and Engineering, Iasi, Romania, 17–18 May 2018; p. 12023. [[CrossRef](#)]
14. Baltatu, M.S.; Vizureanu, P.; Geanta, V.; Nejneru, C.; Tugui, C.A.; Focsaneanu, S.C. Obtaining and Mechanical Properties of Ti-Mo-Zr-Ta Alloys. In Proceedings of the IOP Conference Series: Materials Science and Engineering, Iasi, Romania, 25–26 May 2017; p. 12019. [[CrossRef](#)]
15. Kirmanidou, Y.; Sidira, M.; Drosou, M.E.; Bennani, V.; Bakopoulou, A.; Tsouknidas, A.; Michailidis, N.; Michalakis, K. New Ti-Alloys and Surface Modifications to Improve the Mechanical Properties and the Biological Response to Orthopedic and Dental Implants: A Review. *BioMed Res. Int.* **2016**, *2016*, 2908570. [[CrossRef](#)] [[PubMed](#)]
16. Simoes, S. Recent Progress in the Joining of Titanium Alloys to Ceramics. *Metals* **2018**, *8*, 876. [[CrossRef](#)]
17. Feng, J.; Dai, X.; Wang, D.; Li, R.; Cao, J. Microstructure evolution and mechanical properties of ZrO₂/TiAl joints vacuum brazed by Ag-Cu filler metal. *Mater. Sci. Eng. A* **2015**, *639*, 739–746. [[CrossRef](#)]
18. Baltatu, M.S.; Vizureanu, P.; Goanță, V.; Tugui, C.A.; Voiculescu, I. Mechanical tests for Ti-based alloys as new medical materials. In Proceedings of the IOP Conference Series: Materials Science and Engineering, Iasi, Romania, 16–17 May 2019; p. 012029.
19. Gautam, C.; Joyner, J.; Gautam, A.; Rao, J.; Vajtai, R. Zirconia based dental ceramics: Structure, mechanical properties, biocompatibility and applications. *Dalton Trans.* **2016**, *45*, 19194–19215. [[CrossRef](#)]
20. Alghazzawi, T.F.; Janowski, G.M. Effect of liner and porcelain application on zirconia surface structure and composition. *Int. J. Oral Sci.* **2016**, *8*, 164–171. [[CrossRef](#)]
21. Baloyi, N.M.; Popoola, A.P.I.; Pityana, S.L. Laser coating of Zirconium and ZrO₂ composites on Ti6Al4V for biomedical applications. *S. Afr. J. Ind. Eng.* **2014**, *25*, 62–70. [[CrossRef](#)]
22. Li, J.N.; Chen, C.Z. Effect of ZrO₂ (YPSZ) on microstructure characteristic and wear resistance of the Ti3Al/TiC laser-cladded ceramic layer on titanium alloy. *Int. J. Appl. Ceram. Technol.* **2012**, *9*, 947–952. [[CrossRef](#)]
23. Wang, Y.; Li, C.; Jiang, F.; Zhang, J.; An, X. Microstructure and mechanical properties of ultrasonic assisted laser cladding Al₂O₃-ZrO₂ ceramic coating. *Mater. Res. Express* **2019**, *6*, 106563. [[CrossRef](#)]
24. Vilardell, A.M.; Cinca, N.; Garcia-Giralt, N.; Dosta, S.; Cano, I.G.; Nogues, X.; Guilemany, J.M. In-vitro comparison of hydroxyapatite coatings obtained by cold spray and conventional thermal spray technologies. *Mater. Sci. Eng. C* **2020**, *107*, 110306. [[CrossRef](#)]
25. Marquer, M.; Phippon, S.; Faure, L.; Chassaing, G.; Tardelli, J.; Demmou, K. Influence of two APS coatings on the high-speed tribological behavior of a contact between titanium alloys. *Tribol. Int.* **2019**, *136*, 13–22. [[CrossRef](#)]
26. Stern, K.H. *Metallurgical and Ceramic Protective Coatings*; Springer: Dordrecht, The Netherlands, 1996.
27. Chevalier, J.; Gremillard, L.; Deville, S. Low-temperature degradation of zirconia and implications for biomedical implants. *Ann. Rev. Mater. Res.* **2007**, *37*, 1–32. [[CrossRef](#)]
28. Stescu, C.; Chicet, D.L.; Munteanu, C.M.; Istrate, B.; Benchea, M.; Basescu, G.N. Aspects regarding the influence of the processing regime on the surface quality of thermal sprayed coatings. In *IOP Conference Series: Materials Science and Engineering*; IOP Publishing Ltd.: Bristol, UK, 2018; Volume 444, p. 032012. [[CrossRef](#)]
29. Zheng, K.; Li, L.; Dong, Y.; Gao, J.; Hei, H.; Ma, Y.; Zhou, B.; He, Z.; Wang, Y.; Yu, S.; et al. Preparation, microstructure, mechanical properties and biocompatibility of Ta-coated 3Y-TZP ceramic deposited by a plasma surface alloying technique. *Materials* **2020**, *13*, 1265. [[CrossRef](#)]

30. Lupescu, S.; Munteanu, C.; Istrate, B.; Earar, K. The influence of zr on microstructure, mechanical properties and corrosion resistance in Mg-Y-Zr biodegradable alloys. *Rev. Chim.* **2018**, *69*, 3382–3385. [[CrossRef](#)]
31. Hannink, R.H.; Kelly, P.M.; Muddle, B.C. Transformation toughening in zirconia—containing ceramics. *J. Am. Ceram. Soc.* **2010**, *83*, 461–487. [[CrossRef](#)]

Publisher’s Note: MDPI stays neutral with regard to jurisdictional claims in published maps and institutional affiliations.



© 2020 by the authors. Licensee MDPI, Basel, Switzerland. This article is an open access article distributed under the terms and conditions of the Creative Commons Attribution (CC BY) license (<http://creativecommons.org/licenses/by/4.0/>).